Quadrupolar effect in the perovskite manganite $La_{1-x}Sr_xMnO_3$

Hirofumi Hazama, Terutaka Goto, and Yuichi Nemoto
Graduate School of Science and Technology, Niigata University, Niigata 950-2181, Japan

Yasuhide Tomioka
Joint Research Center for Atom Technology (JRCAT), Tsukuba 305-0046, Japan

Atsushi Asamitsu
Cryogenic Center, University of Tokyo, Tokyo 113-0032, Japan

Yoshinori Tokura
Department of Applied Physics, University of Tokyo, Tokyo 113-8656, Japan
and Joint Research Center for Atom Technology (JRCAT), Tsukuba 305-0046, Japan
(Received 25 May 2000)

Elastic properties of the perovskite manganite $La_{1-x}Sr_xMnO_3$ ($x=0.12$, 0.165, 0.3) with both orbital and charge degrees of freedom have been investigated by means of ultrasonic measurements. Above the structural phase transition point $T_s=290$ K for $x=0.12$ and $T_s=310$ K for $x=0.165$, the transverse $(C_{11}-C_{12})/2$ mode with the elastic strain of E_g symmetry exhibits a pronounced softening, while the C_{44} mode with strain of T_{2g} symmetry shows a monotonous increase in lowering temperature. The softening of $(C_{11}-C_{12})/2$ is described in terms of the quadrupolar susceptibility for the coupling between the quadrupolar moment, $O_2^0=(2l_z^2-l_x^2-l_y^2)/\sqrt{3}$ and $O_2^2=l_x^2-l_y^2$, of the $d\gamma$ doublet of the Mn^{3+} ion and the appropriate elastic strain with E_g symmetry. Elastic softenings of $(C_{11}-C_{12})/2$ and C_{44} modes above $T_{co}=145$ K of $x=0.12$ are responsible for the symmetry breaking character of the charge ordering, while a round minimum of the bulk modulus C_B around $T_{co}=100$ K of $x=0.165$ indicates a glass state in charge ordering. The disappearance of the ultrasonic echo signal below $T_{co}=145$ K for $x=0.12$ is ascribed to a considerable sound wave scattering by elastic domains in the triclinic structure.

I. INTRODUCTION

The hole-doped manganese oxides with perovskite structure, $R_{1-x}A_xMnO_3$ (R being trivalent rare-earth ions and A divalent alkaline-earth metal ions), have been already investigated in the 1950s.[1] The ferromagnetism of the hole-doped materials is explained in terms of the double-exchange mechanism mediated by $d\gamma$ carriers of manganese ions.[2–4] The recent discovery of the colossal magnetoresistance in some member of materials has revived interest in strongly correlated electron systems with spin, orbit, and charge degrees of freedom.[5,6] In particular the degenerate $d\gamma$ orbit of the Mn^{3+} ion plays an important role for the insulator-metal transition as well as the colossal magnetoresistance. The orbital ordering of $d\gamma$ orbits in Mn^{3+} ions, which is occasionally accompanied by a structural change, is also important for the magnetic and electric properties of the system.[7,8] Furthermore, the charge degree of freedom associated with Mn^{4+} ions in hole-doped systems leads to a charge ordering[9] due to the Coulomb interaction. The charge ordering affects their magnetic and transport properties.

It is well known that the $3d$ state with orbital degree of freedom ($l=2$) splits into the doublet of $d\gamma$ states with E_g symmetry and triplet of $d\varepsilon$ states with T_{2g} in the cubic crystalline electric field potential. The Mn^{3+} ion located inside the oxide octahedron of the present perovskite compound has the ground $d\varepsilon$ state and the excited $d\gamma$ state at $10Dq \approx 2$ eV. All spins of $3d$ orbits in Mn^{3+} ions align parallel by large Hund rules coupling. This means that one of the degenerate $d\gamma$ states, $d(3z^2-r^2)$ and $d(x^2-y^2)$, in Mn^{3+} ions is occupied by an electron with spin $S=1/2$, which is parallel to the spin with $S=3/2$ of the $d\varepsilon$ state.

The degeneracy of the $d\gamma$ state in Mn^{3+} ions gives rise to orbital ordering, namely, quadrupolar ordering, in addition to magnetic ordering due to the spin degeneracy.[10–12] Actually the end material $LaMnO_3$ characterized by a Mott insulator exhibits an orbital ordering of the $d\gamma$ state.[13,14] The antiferromagnetism of type A with wave vector $k=[0,0,1/2]$ below $T_N=141$ K in $LaMnO_3$ appears in the orbital-ordered state of type C with alternative orientations of $d(3x^2-r^2)$ and $d(3y^2-r^2)$ in the a-c plane and parallel orientation along the b axis. In the hole-doped compound $La_{1-x}Sr_xMnO_3$, the ferromagnetic double-exchange interaction due to itinerant $d\gamma$ orbit surpasses the antiferromagnetic superexchange interaction of the localized $d\gamma$ orbit via oxygen. The contribution of the orbital degree of freedom to the colossal magnetoresistance in $La_{1-x}Sr_xMnO_3$ systems is the main issue to be clarified.

The $3d$ electron of transition-metal ions has an electric quadrupolar moment due to the orbital state as well as a magnetic dipole moment associated with the spin degree of freedom. Therefore the $3d$ state of transition-metal ions is perturbed by a modulation of the crystalline electric field potential due to the lattice vibration. The coupling of the

quadrupolar moment of the $3d$ electron to the lattice degree of freedom gives rise to anomalies of the ultrasonic wave. This is called the Jahn-Teller effect. The elastic anomalies due to the quadrupolar ordering refer to $NiCr_2O_4$ (Refs. 15 and 16) and $CsCuCl_3$ (Ref. 17). A model calculation taking into account the electron-lattice interaction was proposed to explain the colossal magnetoresistance of the manganese compounds.[18] Previous ultrasonic studies focusing on the electron-lattice interaction of manganese compounds have been done.[19,20] In order to examine the electron-lattice interaction quantitatively, we have made a systematic investigation of the elastic constants of $La_{1-x}Sr_xMnO_3$ ($x=0.12,0.165,0.3$) by means of ultrasonic measurements.

The charge degree of freedom associated with the doped Mn^{4+} ions in a sea of Mn^{3+} couples with the elastic strain due to the sound wave. The coupling of the charge fluctuation mode to the elastic strain gives rise to the softening of the elastic constant around the charge ordering point. The softening of the C_{44} mode in the magnetite Fe_3O_4 (Ref. 21) associated with the charge fluctuation between Fe^{2+} and Fe^{3+} ions and the rare-earth pnictide Yb_4As_3 (Ref. 22) with the fluctuation mode between Yb^{2+} and Yb^{3+} ions was well investigated by the ultrasonic method. The clarification of the elastic anomalies due to the charge ordering in $x=0.12$ and 0.165 compounds is also the issue of the present paper.

In the next section we describe the experimental procedure of the present study. The quadrupole-strain interaction for the $d\gamma$ orbit of Mn^{3+} ions is briefly mentioned in Sec. III. The temperature dependences of the elastic constants of $x=0.12$ and 0.165 with cubic geometry are shown in Secs. IV A and IV B, respectively. The temperature and field dependences of the elastic constants for $x=0.165$ and 0.3 with rhombohedral geometry are shown in Sec. IV C. The conclusion is mentioned in Sec. V.

II. EXPERIMENT

Crystals of $La_{1-x}Sr_xMnO_3$ used in the present ultrasonic measurements were grown by a floating zone (FZ) furnace equipped with a halogen lamp and ellipsoidal mirror. The starting materials La_2O_3, $SrCO_3$, and Mn_3O_4 were weighted to be of stoichiometric amount. The orientation of the grown crystals was determined by an x-ray camera and prepared by a cutter with a diamond tooth. The mosaicness in the pseudocubic phase O* of the present $x=0.12$ sample was less than 0.3°. The surfaces of oriented crystal were polished carefully to be plane parallel. The ultrasonic transducers of $LiNbO_3$ plates bonded on the parallel surfaces were used for the generator and detector of the ultrasonic pulse wave. The sound velocity v as a function of temperature and magnetic field was measured by a homemade apparatus based on the phase comparison method. The elastic constant is obtained as $C=\rho v^2$; here ρ is the mass density of the material.

A magnetic field up to 80 kOe was generated by a superconducting magnet. The axes of orthorhombic phase (pseudocubic phase O* and Jahn-Teller distorted phase O′) and rhombohedral phase R are shown in Figs. 1(a) and 1(b), respectively. The b axis of the orthorhombic phase coincides with the prototype cubic z axis, but the a and c axes orientate to the direction with angle of 45° to x and y axes of prototype cubic structure. It should be noted that the principal Z axis of the rhombohedral crystal R coincides with the body diagonal [111] direction of the cubic one. The X and Y axes of the rhombohedral crystal R in Fig. 1(b) are parallel to the $[11\bar{2}]$ and $[1\bar{1}0]$ directions of the cubic one, respectively. We argue the symmetry of the quadrupolar operators, the elastic strains, and the elastic constants in the orthorhombic and rhombohedral crystals by use of the crystal axes in Figs. 1(a) and 1(b).

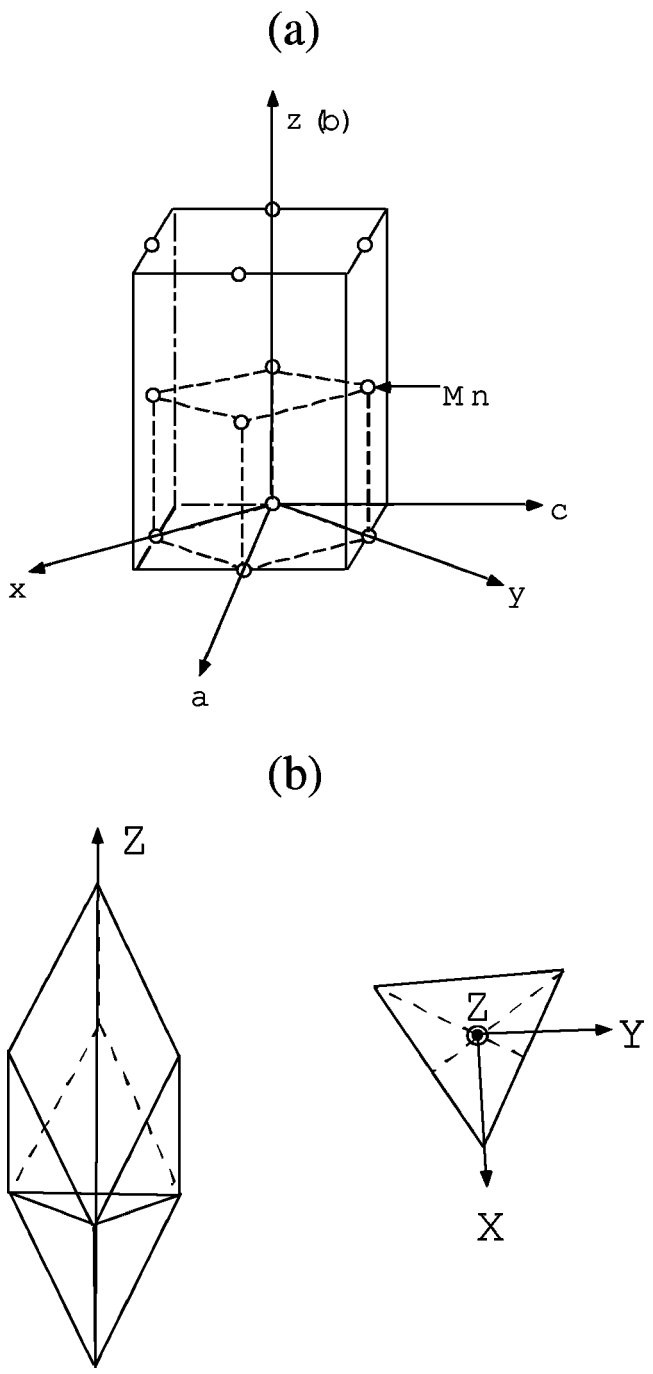

FIG. 1. (a) a,b,c axes of orthorhombic O* and O′ phase in $x=0.12$ and 0.165. Here x,y,z axes mean the crystal axes of the prototype cubic phase. (b) X,Y,Z axes of the rhombohedral phase in $x=0.165$ and 0.3.

TABLE I. The quadrupolar operators, elastic strains, and elastic constants classified by irreducible representations in cubic symmetry. The elastic strain is defined as $\varepsilon_{\alpha\beta}=\frac{1}{2}(\partial u_\beta/\partial\alpha+\partial u_\alpha/\partial\beta)$; here α,β mean the coordinates x,y,z defined for the axes of the cubic phase in Fig. 1(a). And l_x, l_y, and l_z mean the angular momentum.

Symmetry	Quadrupolar moment	Elastic strain	Elastic constant
A_{1g}	$O_B=l_x^2+l_y^2+l_z^2$	$\varepsilon_B=\varepsilon_{xx}+\varepsilon_{yy}+\varepsilon_{zz}$	$(C_{11}+2C_{12})/3$
E_g	$O_2^0=(2l_z^2-l_x^2-l_y^2)/\sqrt{3}$	$\varepsilon_u=(2\varepsilon_{zz}-\varepsilon_{xx}-\varepsilon_{yy})/\sqrt{3}$	$(C_{11}-C_{12})/2$
	$O_2^2=l_x^2-l_y^2$	$\varepsilon_v=\varepsilon_{xx}-\varepsilon_{yy}$	
T_{2g}	$O_{yz}=l_yl_z+l_zl_y$	ε_{yz}	C_{44}
	$O_{zx}=l_zl_x+l_xl_z$	ε_{zx}	
	$O_{xy}=l_xl_y+l_yl_x$	ε_{xy}	

III. QUADRUPOLE-STRAIN INTERACTION

The $3d$ orbits of manganese ions in the present perovskite compounds split into the ground-state $d\varepsilon$ triplet and excited $d\gamma$ doublet at $10Dq\approx 2$ eV. In Mn^{3+} ions with $3d^4$ configuration, one of the degenerate $d\gamma$ states is occupied by an electron with $S=1/2$ parallel to the spin $S=3/2$ of $d\varepsilon$ states. The $d\gamma$ electron in the $3d^3$ state of Mn^{4+} ions has a tiny population at room temperature. Therefore the quadrupolar moment of the $d\gamma$ state is responsible for Mn^{3+} ions, but is practically absent for Mn^{4+} ions. In order to describe the quadrupole-strain interaction, we employ quadrupolar operators as $O_2^0=(2l_z^2-l_x^2-l_y^2)/\sqrt{3}$, $O_2^2=l_x^2-l_y^2$ with E_g symmetry and $O_{yz}=l_yl_z+l_zl_y$, $O_{zx}=l_zl_x+l_xl_z$, $O_{xy}=l_xl_y+l_yl_x$ with T_{2g} symmetry. Here l_x, l_y, and l_z mean the components of the angular momentum. The elastic strain of the cubic crystal class is described in terms of the volume strain $\varepsilon_B=\varepsilon_{xx}+\varepsilon_{yy}+\varepsilon_{zz}$ with A_{1g} symmetry, $\varepsilon_u=(2\varepsilon_{zz}-\varepsilon_{xx}-\varepsilon_{yy})/\sqrt{3}$, $\varepsilon_v=\varepsilon_{xx}-\varepsilon_{yy}$ with E_g, and ε_{yz}, ε_{zx}, ε_{xy} with T_{2g}. The transverse $(C_{11}-C_{12})/2$ mode propagating along [110] with polarization parallel to $[1\bar{1}0]$ induces the elastic strain $\varepsilon_v=\varepsilon_{xx}-\varepsilon_{yy}$ of one part of the E_g representation. The transverse C_{44} mode, which propagates along the [100] direction with the polarization parallel to [010], induces the strain ε_{xy} of the T_{2g} representation. The symmetry of the quadrupolar operators, the elastic strains, and the corresponding elastic constants in cubic crystal are presented in Table I.

The modulation of the crystal field potential for Mn^{3+} ions by the external strain $\varepsilon_{\Gamma\gamma}$ of the sound wave is written as[8,10,16]

$$H_{QS}=-\sum_i\sum_{\Gamma\gamma} g_\Gamma O_{\Gamma\gamma}(i)\varepsilon_{\Gamma\gamma}. \tag{1}$$

Here g_Γ is a coupling constant and $O_{\Gamma\gamma}(i)$ is the quadrupolar operator of the manganese ion at the ith site. The intersite interaction of the quadrupolar moment is taken into account as

$$H_{QQ}=-\sum_i\sum_{\Gamma\gamma} g'_\Gamma\langle O_{\Gamma\gamma}\rangle O_{\Gamma\gamma}(i). \tag{2}$$

Here $\langle O_{\Gamma\gamma}\rangle$ represents a mean-field value of the quadrupoler momentum and g'_Γ is a coupling constant of the intersite quadrupolar interaction. The elastic constant $C_\Gamma(T)$ as a function of temperature is written as

$$C_\Gamma(T)=C_\Gamma^0-Ng_\Gamma^2\frac{\chi_\Gamma(T)}{1-g'_\Gamma\chi_\Gamma(T)}. \tag{3}$$

Here N is the number of Mn^{3+} ions in unit volume and $\chi_\Gamma(T)$ is the quadrupolar susceptibility for a Mn^{3+} ion. When the ground state has a quadrupolar moment in the diagonal element as $\langle\varphi_i|O_{\Gamma\gamma}|\varphi_i\rangle$, the quadrupolar susceptibility is dominated by the Curie term $\chi_\Gamma(T)=|\langle\varphi_i|O_{\Gamma\gamma}|\varphi_i\rangle|^2/T$ at low temperatures. Then the elastic constant of Eq. (3) is written as

$$C_\Gamma(T)=C_\Gamma^0\left(\frac{T-T_c^0}{T-\Theta}\right). \tag{4}$$

Here the characteristic temperatures of T_c^0 and Θ are determined by the ultrasonic measurements of the elastic softening. It should be noted that $\Theta=g'_\Gamma|\langle\varphi_i|O_{\Gamma\gamma}|\varphi_i\rangle|^2$ indicates the intersite quadrupolar coupling. The Jahn-Teller coupling energy for the bulk strain $E_{JT}=Ng_\Gamma^2|\langle\varphi_i|O_{\Gamma\gamma}|\varphi_i\rangle|^2/C_\Gamma^0$ is obtained by the difference of two characteristic temperatures as $T_c^0-\Theta=E_{JT}$.[8]

The $d\gamma$ state of Mn^{3+} ions has the quadrupolar moment of O_2^0 and O_2^2 with E_g symmetry, $|\langle\varphi_{e_g}|O_{\Gamma\gamma}|\varphi_{e_g}\rangle|=2\sqrt{3}$. The $|\varphi_{e_g}\rangle$ means the wave function of the $d\gamma$ electron, $\varphi_u=d(3z^2-r^2)$ and $\varphi_v=d(x^2-y^2)$, with E_g symmetry in the cubic structure. But the quadrupolar moment O_{xy} with T_{2g} symmetry is absent for the $d\gamma$ state, $|\langle\varphi_{e_g}|O_{xy}|\varphi_{e_g}\rangle|=0$. This simple argument of the quadrupolar moment promises that the $(C_{11}-C_{12})/2$ mode responsible for O_2^0 or O_2^2 shows a softening due to the Curie term, $\chi_\Gamma(T)=(2\sqrt{3})^2/k_BT$, in the quadrupolar susceptibility of Eq. (3). In the case of the C_{44} mode for the response of O_{xy}, however, the absence of the Curie term leads to a normal increase of C_{44} in lowering temperature. The formula explained above is used even in the case of lower symmetry for the rhombohedral structure of the present compound $La_{1-x}Sr_xMnO_3$. In Table II we list the quadrupolar operators, the elastic strains, and the elastic constants defined in the rhombohedral structure.

IV. RESULTS AND DISCUSSIONS

A. Elastic constant of $x=0.12$: Cubic geometry

We show the temperature dependence of the elastic constants for the $x=0.12$ ($\approx 1/8$) compound in Fig. 2. In the measurements of the sound velocity we used ultrasonic

TABLE II. The quadrupolar operators, elastic strains, and elastic constants classified by irreducible representations in rhombohedral symmetry. The coordinates x,y,z are defined for the rhombohedral axes X,Y,Z of Fig. 1(b).

Symmetry	Quadrupolar moment	Elastic strain	Elastic constant
A_{1g}	$O_B=l_x^2+l_y^2+l_z^2$	$\varepsilon_B=\varepsilon_{xx}+\varepsilon_{yy}+\varepsilon_{zz}$	$(2C_{11}^{Rhom}+2C_{12}^{Rhom}-C_{33}^{Rhom})/3$
	$O_2^0=(2l_z^2-l_x^2-l_y^2)/\sqrt{3}$	$\varepsilon_u=(2\varepsilon_{zz}-\varepsilon_{xx}-\varepsilon_{yy})/\sqrt{3}$	$(2C_{33}^{Rhom}-C_{11}^{Rhom}-C_{12}^{Rhom})/2$
E_g	$O_{yz}=l_yl_z+l_zl_y$	ε_{yz}	C_{44}^{Rhom}
	$O_{zx}=l_zl_x+l_xl_z$	ε_{zx}	
	$O_2^2=l_x^2-l_y^2$	$\varepsilon_v=\varepsilon_{xx}-\varepsilon_{yy}$	$C_{66}^{Rhom}=(C_{11}^{Rhom}-C_{12}^{Rhom})/2$
	$O_{xy}=l_xl_y+l_yl_x$	ε_{xy}	

waves with frequencies 10–30 MHz. The directions of propagation and polarization of the ultrasonic waves are oriented to the axes of the prototype cubic structure. The notation of C_{ij} in Fig. 2 follows the definition of the cubic crystal in Table I. The mosaicness less than 0.3° in the pseudocubic phase O* has little influence on the mode mixing of the acoustic waves. The bulk modulus $C_B=(C_{11}+2C_{12})/3$ is obtained by the result of $(C_{11}-C_{12})/2$ and C_{11} in Fig. 2. It should be noted that the $(C_{11}-C_{12})/2$ mode exhibits a softening of 30% in the O* phase above $T_s=290$ K, while the C_{44} mode shows a monotonous increase. The bulk modulus C_B also increases monotonously above T_s.

The softening of $(C_{11}-C_{12})/2$ above T_s in Fig. 2 is attributed to the Curie term in the quadrupolar susceptibility of O_2^0 or O_2^2 for the $d\gamma$ state of Mn^{3+} ion. In Fig. 3, we present again the softening of $(C_{11}-C_{12})/2$ in expanded scales. The solid line of Fig. 3 indicates the calculated result by Eq. (3) with the quadrupole-strain coupling constant $|g_{\Gamma 3}|=1167$ K and the ferrotype quadrupolar intersite coupling $g'_{\Gamma 3}=16$ K >0. The dashed line in Fig. 3 means a background part. This fitting leads the characteristic temperatures $T_c^0=240$ K and $\Theta=188$ K in Eq. (4). It is noticeable that the Jahn-Teller coupling energy $E_{JT}=52$ K is comparable to the intersite quadrupolar interaction $\Theta=188$ K.

It is naturally expected that a sizable softening of $(C_{11}-C_{12})/2$ gives rise to the quadrupolar ordering of the O_2^0- or O_2^2-type moment below T_s. The ordering of O_2^0 at the Γ point of the Brillouin zone results in spontaneous tetragonal distortion as

$$\langle \varepsilon_u \rangle = \frac{N g_{\Gamma 3}}{(C_{11}^0-C_{12}^0)/2}\langle O_2^0 \rangle. \tag{5}$$

The parameters $N=1.5\times10^{22}$ cm^{-3}, $|g_{\Gamma 3}|=1167$ K, and $(C_{11}^0-C_{12}^0)/2=6.5\times10^{11}$ erg/cm^3 obtained by ultrasonic measurements lead to tetragonal distortion $\langle \varepsilon_u \rangle \approx \pm 1.29\times10^{-2}$. The sign of the distortion remains to be determined. Kawano *et al.* have already measured the lattice parameter of $x=0.125$ around the structural transition.[23] The pseudocubic

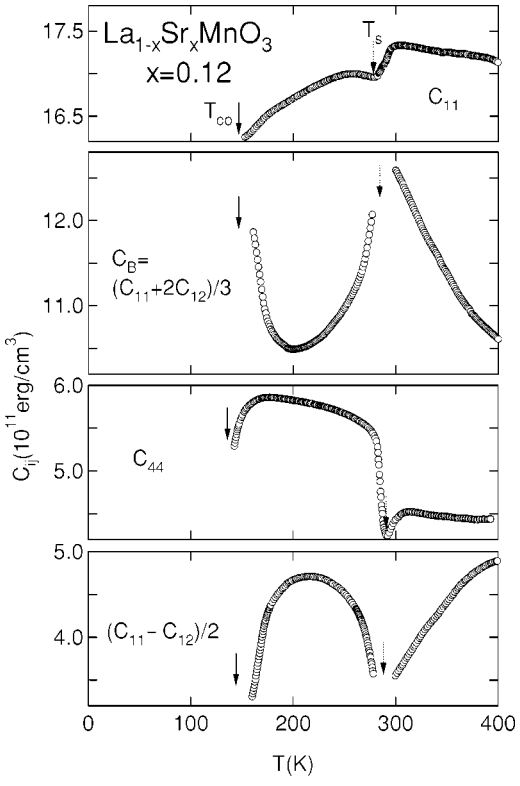

FIG. 2. Temperature dependence of the elastic constants in $La_{0.88}Sr_{0.12}MnO_3$. The elastic softening of the transverse $(C_{11}-C_{12})/2$ mode has been found above the structural phase transition point $T_s=290$ K. The elastic constants $(C_{11}-C_{12})/2$ and C_{44} exhibit remarkable softening above the charge ordering point $T_{co}=145$ K due to the charge fluctuation of Mn^{4+} ions in a sea of Mn^{3+} ions.

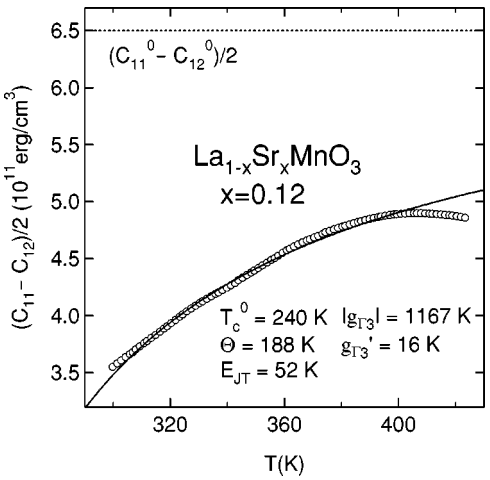

FIG. 3. The elastic softening of the transverse $(C_{11}-C_{12})/2$ mode above $T_s=290$ K in $La_{0.88}Sr_{0.12}MnO_3$. The solid line is a calculated curve by Eq. (4) with $T_c^0=240$ K and $\Theta=188$ K. Here we obtain the parameters $|g_{\Gamma 3}|=1167$ K, $g'_{\Gamma 3}=16$ K>0, and $E_{JT}=52$ K. The dashed line is a background part of $(C_{11}^0-C_{12}^0)/2$.

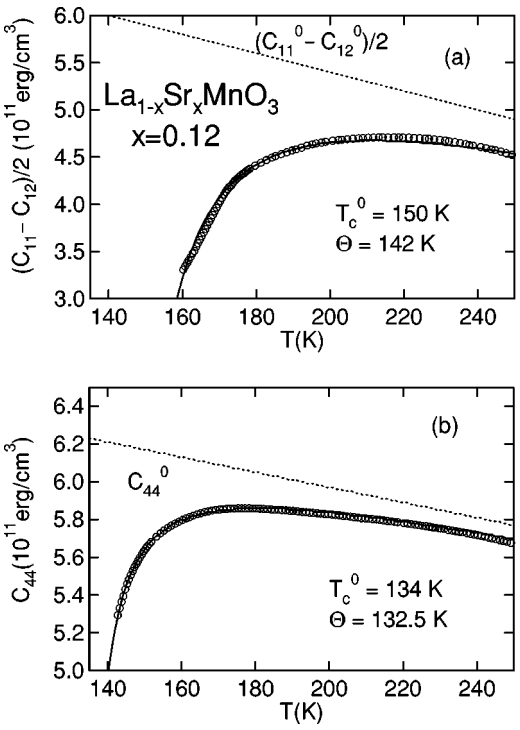

FIG. 4. (a) The elastic softening of the transverse $(C_{11}-C_{12})/2$ mode above $T_{co}=145$ K in $La_{0.88}Sr_{0.12}MnO_3$. The solid line is a calculated curve by Eq. (4) with $T_c^0=150$ K and $\Theta=142$ K. The dashed line is a background part of $(C_{11}^0-C_{12}^0)/2$. (b) The elastic softening of the transverse C_{44} mode. The solid line is a calculated curve with $T_c^0=134$ K and $\Theta=132.5$ K. The dashed line is a background part of C_{44}^0.

phase O* with $a=5.537$ Å, $b/\sqrt{2}=5.530$ Å, and $c=5.545$ Å is characterized as a deformed lattice with $\langle\varepsilon_u\rangle=-2.29\times10^{-3}$ and $\langle\varepsilon_v\rangle=-1.44\times10^{-3}$ from a hypothetical cubic lattice with $a=5.537$ Å. The parameters $a=5.561$ Å, $b/\sqrt{2}=5.489$ Å, and $c=5.556$ Å in the O′ phase below T_s are characterized by deformations of $\langle\varepsilon_u\rangle=-1.45\times10^{-2}$ and $\langle\varepsilon_v\rangle=9.03\times10^{-4}$ from hypothetical cubic lattices. The spontaneous distortion $\langle\varepsilon_u\rangle=-1.22\times10^{-2}$ across the transition from O* to O′ obtained by the neutron measurement means shrinkage along the z direction and elongation along the x and y directions. This result is well consistent with the result of Eq. (5) for a negative value of $g_{\Gamma3}=-1167$ K of the ultrasonic measurement.

The elastic constants $(C_{11}-C_{12})/2$ and C_{44} of $x=0.12$ in Fig. 2 also show softenings above the charge ordering point $T_{co}=145$ K, while the bulk modulus C_B increases considerably above T_{co}. Those softenings of both shear modes $(C_{11}-C_{12})/2$ and C_{44} are responsible for the coupling of the elastic strain with the symmetry breaking character to the charge fluctuation modes of Mn^{4+} ions in a sea of Mn^{3+} ions. In analogy to the charge ordering of Yb_4As_3, the elastic soft mode is explained by the Eq. (4). Therefore we employed Eq. (4) for the fitting of $(C_{11}-C_{12})/2$ and C_{44} above T_{co} in Figs. 4(a) and 4(b). The characteristic temperatures $T_c^0=134$ K and $\Theta=132.5$ K for C_{44} in Fig. 4(b) are smaller than $T_c^0=150$ K and $\Theta=142$ K for $(C_{11}-C_{12})/2$ in Fig. 4(a). This means that the charge fluctuation mode coupling with $(C_{11}-C_{12})/2$ dominates for the charge ordering in $x=0.12$ in comparing the contribution from the mode coupled with C_{44}.

When the potential energy due to the Coulomb interaction among Mn^{4+} ions in a sea of Mn^{3+} ions is superior to the kinetic energy, the charge ordering is expected in lowering temperature. The coexistence ratio of $N(Mn^{4+}):N(Mn^{3+})=1:7$ in the present $x=0.12\,(\approx1/8)$ compound favors the charge ordering being commensurable with the lattice periodicity. A polaron ordering model has been proposed to explain lattice distortion associated with the charge ordering of Mn^{4+} ions in low doped $x=0.10$ and $x=0.15$ compounds.[10] However, the relationship of the charge ordering to the softenings in $(C_{11}-C_{12})/2$ and C_{44} is not clear at the present stage. The peak intensity of the resonant x-ray scattering of $x=0.12$ increases considerably below 145 K.[24] They interpret the result as orbital ordering below 145 K. The interplay of the orbital ordering to the elastic softenings in the present ultrasonic measurement above T_{co} remains to be solved.

The sound echo completely disappears below T_{co} because of the sound wave scattering by the elastic domain walls in the charge ordered phase with a low-symmetry crystal class, probably a triclinic one.[24] This unusual disappearance of the ultrasonic echo signal in the O* phase below T_{co} differs from the behavior of the O* phase above T_s. The reentrant model is unrealistic for the O* phase below T_{co} in the present $x=0.12$ compound. The ferromagnetic transition point $T_C=170$ K was observed by magnetic and transport measurements. In the present result, however, the indication of the ferromagnetic transition is obscure.

B. Elastic constant of $x=0.165$: Cubic geometry

In Fig. 5 we show the temperature dependence of the elastic constants of $x=0.165$, which is characterized by the colossal magnetoresistance. The ultrasonic measurement has been done in accordance with the crystallographic axes of the prototype cubic structure. It is noticeable that the transverse $(C_{11}-C_{12})/2$ mode associated with the elastic strain $\varepsilon_u=(2\varepsilon_{zz}-\varepsilon_{xx}-\varepsilon_{yy})/\sqrt{3}$ with E_g symmetry exhibits a softening in the rhombohedral phase above the structural transition $T_s=310$ K. On the other hand, the transverse C_{44} mode, longitudinal C_{11} mode, and bulk modulus C_B increase as the temperature is lowered to T_s.

This characteristic softening of $(C_{11}-C_{12})/2$ in the rhombohedral phase above T_s is again attributed to the quadrupolar susceptibility of O_2^0 or O_2^2 for the $d\gamma$ doublet of Mn^{3+} ions. The increase of C_{44} above T_s is also consistent with the absence of the quadrupolar moment O_{xy} for the $d\gamma$ doublet of Mn^{3+}. Using the quadrupolar susceptibility in Eq. (3), we obtained the solid line in Fig. 6. The coupling constant $|g_{\Gamma3}|=496$ K for $x=0.165$ is smaller than the result $|g_{\Gamma3}|=1167$ K of $x=0.12$ in Fig. 3. It has been found that the intersite quadrupolar interaction of $x=0.165$ is $g'_{\Gamma3}=15$ K >0 for the softening of $(C_{11}-C_{12})/2$ in Fig. 6. The characteristic temperatures $T_c^0=190$ K and $\Theta=175$ K are obtained. It is noticeable that the Jahn-Teller coupling energy $E_{JT}=T_c^0-\Theta=15$ K of $x=0.165$ is smaller than $E_{JT}=52$ K for $x=0.12$.

The elastic constants of $x=0.165$ in Fig. 5 exhibit obvious anomalies at the ferromagnetic transition point at $T_C=260$ K. Below T_C the resistivity of $x=0.165$ reduces very much due to the insulator-metal transition.[25] It has already been pointed out that Mn^{4+} ions in a sea of Mn^{3+} ions in

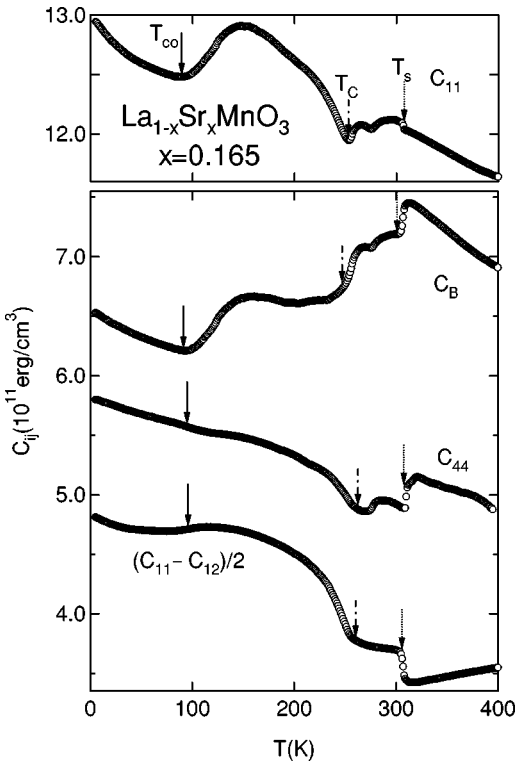

FIG. 5. Temperature dependence of the elastic constants in the cubic geometry of $La_{0.835}Sr_{0.165}MnO_3$. The elastic softening of the transverse $(C_{11}-C_{12})/2$ mode above the structural phase transition point $T_s=310$ K has been found. The anomalies of the ferromagnetic transition $T_C=260$ K and charge ordering point $T_{co}=100$ K are revealed.

$x=0.165$ show charge ordering around $T_{co}=100$ K. Actually the longitudinal C_{11} mode and the bulk modulus C_B in Fig. 5 exhibit round minima around $T_{co}=100$ K. The transverse $(C_{11}-C_{12})/2$ and C_{44} modes, however, show few anomalies around T_{co}. This behavior is contrast to the remarkable softening in the symmetry breaking elastic modes

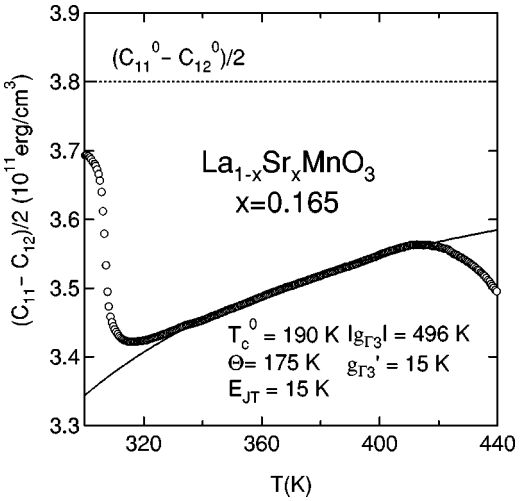

FIG. 6. The elastic softening of the transverse $(C_{11}-C_{12})/2$ mode above $T_s=310$ K in $La_{0.835}Sr_{0.165}MnO_3$. The solid line is a calculated curve by Eq. (4) with $T_c^0=190$ K and $\Theta=175$ K. Here we obtain the parameters $|g_{\Gamma 3}|=496$ K, $g'_{\Gamma 3}=15$ K>0, and $E_{JT}=15$ K. The dashed line is a background part of $(C_{11}^0-C_{12}^0)/2$.

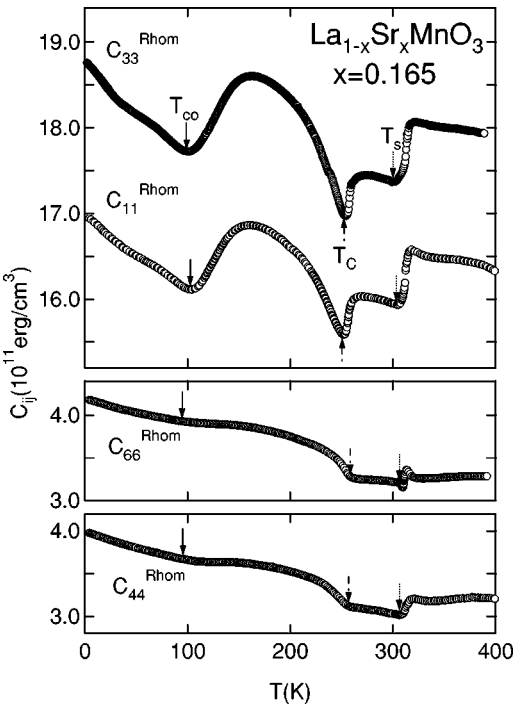

FIG. 7. Temperature dependence of the elastic constants in the rhombohedral geometry of $La_{0.835}Sr_{0.165}MnO_3$. The elastic softenings of the transverse C_{44}^{Rhom} and C_{66}^{Rhom} modes have been found above the structural phase transition point $T_s=310$ K. The elastic anomalies have been found around the ferromagnetic transition $T_C=260$ K and charge ordering point $T_{co}=100$ K.

$(C_{11}-C_{12})/2$ and C_{44}, which has been observed in the present system of $x=0.12$ and the inhomogeneous valence fluctuation compound Yb_4As_3 (Ref. 22) and Fe_3O_4 (Ref. 21). The anomaly around T_{co} of the bulk modulus C_B associated with the total symmetric volume strain may suggest a glass character of the charge ordering in the present $x=0.165$ compound. The elastic anomaly of the longitudinal ultrasonic wave has been found for the mixed crystal systems of $Yb_4(As_{1-x}Sb_x)_3$ (Ref. 26) and $(KBr)_{1-x}(KCN)_x$ (Ref. 27). The incommensurability of the arrangement of the doped Mn^{4+} ions to the lattice periodicity gives rise to the charge glass transition at T_{co}. Furthermore, the screening effect due to the carrier of the $d\gamma$ electrons prevents symmetry-breaking-type charge ordering and favors rather glass behavior.

C. Elastic constant of $x=0.165$ and 0.3: Rhombohedral geometry

In Secs. IV A and IV B we present the elastic constants of $x=0.12$ and 0.165 using the notation of a cubic crystal. However, the rhombohedral structure above $T_s=310$ K of $x=0.165$ with angle $\alpha\approx 61°$ is considerably distorted from the prototype cubic crystal. Therefore it is also important to examine the elastic constants in the geometry of rhombohedral crystal class. In Fig. 7 we show the temperature dependence of the elastic constants of $x=0.165$ in the rhombohedral geometry. The C_{11}^{Rhom} and C_{33}^{Rhom} were measured by the longitudinal sound waves propagating along X and Z axes of the rhombohedral crystal as shown in Fig. 1. Both C_{11}^{Rhom} and C_{33}^{Rhom} show anomalies around the successive phase transi-

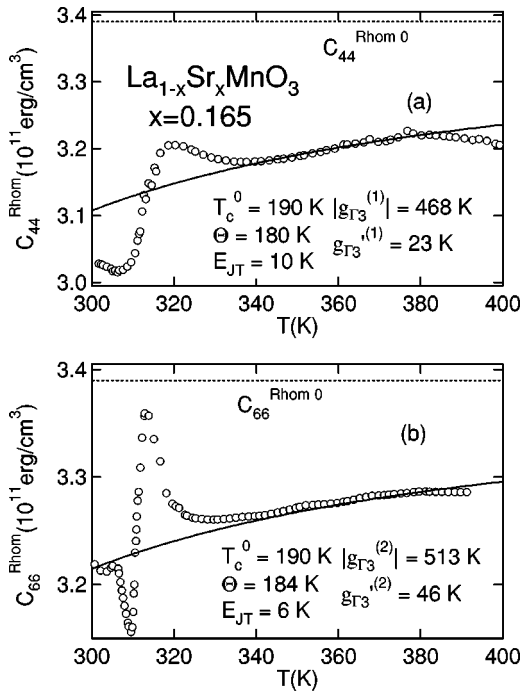

FIG. 8. (a) The elastic softening of the transverse C_{44}^{Rhom} mode in the rhombohedral geometry above $T_s=310$ K in $La_{0.835}Sr_{0.165}MnO_3$. The solid line is a calculated curve by Eq. (4) with $T_c^0=190$ K and $\Theta=180$ K. Here we obtain parameters $|g_{\Gamma 3}^{(1)}|=468$ K, $g'_{\Gamma 3}{}^{(1)}=23$ K>0, and $E_{JT}=10$ K. The dashed line is a background part of C_{44}^{Rhom0}. (b) The elastic softening of the transverse C_{66}^{Rhom} mode. The solid line is a calculated curve with $T_c^0=190$ K and $\Theta=184$ K. Here we obtain parameters $|g_{\Gamma 3}^{(2)}|=513$ K, $g'_{\Gamma 3}{}^{(2)}=46$ K>0, and $E_{JT}=6$ K. The dashed line is a background part of C_{66}^{Rhom0}.

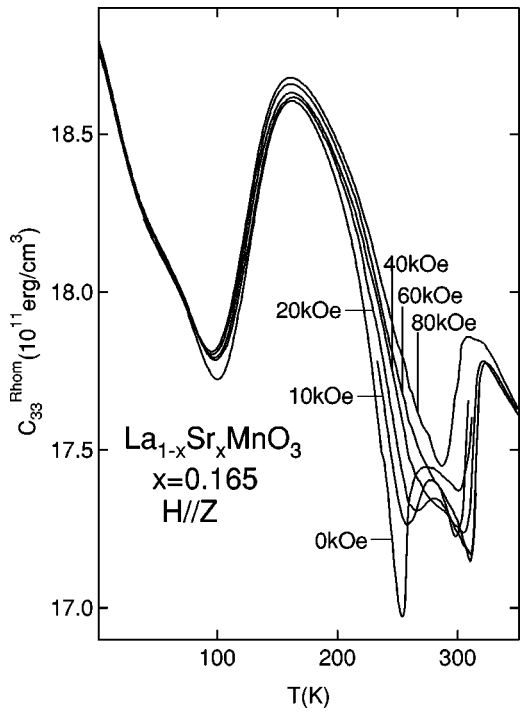

FIG. 9. Temperature dependence of the elastic constant C_{33}^{Rhom} in the rhombohedral geometry of the manganese compound $La_{0.835}Sr_{0.165}MnO_3$ under the magnetic field along Z axis of the principal direction.

tions, structural transition $T_s=310$ K, ferromagnetic transition $T_C=260$ K, and charge ordering $T_{co}=100$ K. The transverse modes C_{44}^{Rhom} and C_{66}^{Rhom} in Fig. 7 also show anomalies around the structural transition T_s and ferromagnetic transition T_C, but exhibit few anomalies at the charge ordering point T_{co}.

It is necessary to take into account the lower-symmetry point group D_{3d} for the rhombohedral structure for the calculation of the quadrupolar susceptibility of Mn^{3+} ions in $x=0.165$. The compatible relation of group theory shows that the degeneracy of $d\gamma$ doublet of Mn^{3+} ions remains even in the rhombohedral structure. The quadrupolar moment O_{yz} with a diagonal element $|\langle\varphi_{e_g}^{Rhom}|O_{yz}|\varphi_{e_g}^{Rhom}\rangle|=2\sqrt{2}$ gives rise to the Curie term of the quadrupolar susceptibility for C_{44}^{Rhom}. The $|\varphi_{e_g}^{Rhom}\rangle$ means the wave function of the $d\gamma$ electron, $\varphi_{u+}=-(\varphi_u+i\varphi_v)/\sqrt{2}$ and $\varphi_{u-}=(\varphi_u-i\varphi_v)/\sqrt{2}$, of E_g symmetry in the rhombohedral structure with D_{3d}. The softening of C_{44}^{Rhom} in Fig. 8(a) is well explained by the coupling constants $|g_{\Gamma 3}^{(1)}|=468$ K and $g'_{\Gamma 3}{}^{(1)}=23$ K. This result leads to the characteristic temperatures being $T_c^0=190$ K, $\Theta=180$ K, and the Jahn-Teller energy $E_{JT}=10$ K.

Furthermore, the quadrupolar moment O_2^2 connecting with C_{66}^{Rhom} has $|\langle\varphi_{e_g}^{Rhom}|O_2^2|\varphi_{e_g}^{Rhom}\rangle|=2$ in the diagonal element. The transverse C_{66}^{Rhom} mode, which is equivalent to the $(C_{11}^{Rhom}-C_{12}^{Rhom})/2$ mode in rhombohedral structure, is expected to decrease due to the Curie term in the quadrupolar susceptibility. The result of Fig. 8(b) shows that the elastic softening of C_{66}^{Rhom} above T_s in $x=0.165$ is explained in terms of the quadrupolar susceptibility with $|g_{\Gamma 3}^{(2)}|=512$ K and $g'_{\Gamma 3}{}^{(2)}=46$ K>0. The characteristic temperatures are $T_c^0=190$ K, $\Theta=184$ K, and the Jahn-Teller energy $E_{JT}=6$ K. It should be noted that the strengths of the quadrupole-strain interaction $|g_{\Gamma 3}|=400$–600 K in Figs. 8(a) and 8(b) are comparable to the result in Fig. 6 based on the cubic geometry. Furthermore, the characteristic temperatures and the coupling energy are almost consistent with the values in the cubic geometry. The anomalous enhancements of C_{44}^{Rhom} in Fig. 8(a) and C_{66}^{Rhom} in Fig. 8(b) have been commonly found above the structural transition point $T_s=310$ K. The origin of those behaviors is not clear and not explained by the quadrupole-strain interaction.

In order to shed light on the colossal magnetoresistance, the measurement of the field dependence of the elastic constant is of great importance. In Fig. 9 we present the longitudinal C_{33}^{Rhom} mode applying the field parallel to its propagating direction of the rhombohedral Z axis. The elastic anomalies associated with both structural and ferromagnetic transitions reveal considerable field dependence, which coincides with the colossal magnetoresistance. The round minimum around charge ordering shows a relatively small field dependence.

In Fig. 10, we show the magnetic phase diagram of $x=0.165$ determined by the present ultrasonic measurement. ''O'' ahead of the hyphen means orthorhombic phase and ''R'' means rhombohedral phase. ''Para'' behind the hyphen shows the paramagnetic phase, ''Ferro'' shows the ferromag-

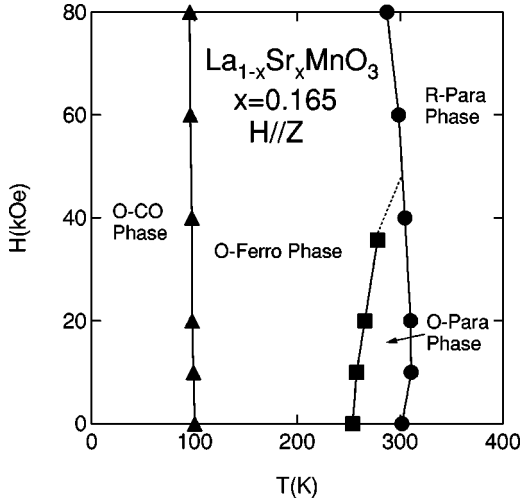

FIG. 10. The magnetic phase diagram of $La_{0.835}Sr_{0.165}MnO_3$. The field is applied along the Z axis of the rhombohedral geometry. ''O'' ahead of the hyphen means orthorhombic phase and ''R'' means rhombohedral phase. ''Para'' behind the hyphen shows the paramagnetic phase, ''Ferro'' shows the ferromagnetic phase, and ''CO'' shows the charge ordering phase.

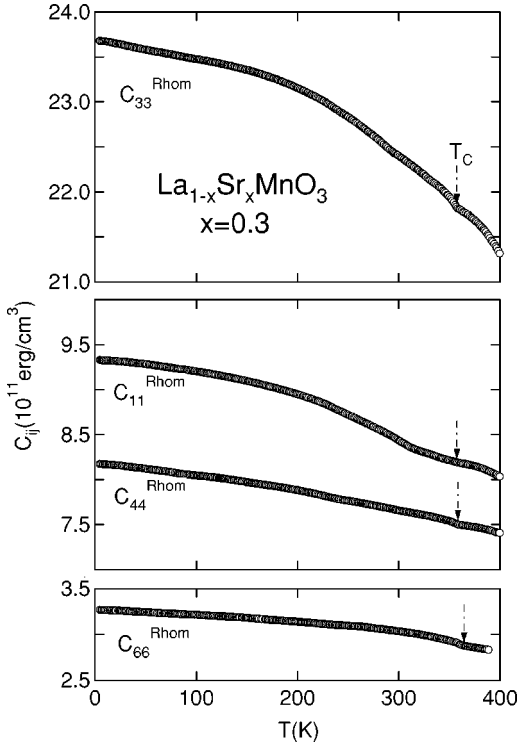

FIG. 11. Temperature dependence of the elastic constants in the rhombohedral geometry of the manganese compound $La_{0.7}Sr_{0.3}MnO_3$. No softening of the elastic constant has been found.

netic phase, and ''CO'' shows the charge ordering phase. The poor field dependence of the charge ordering point means that the charge degree of freedom is unaffected by the external magnetic field. In contrast to that the structural transition point decreases remarkably in increasing field. Furthermore, the ferromagnetic transition point increases considerably in increasing field. The ferromagnetic anomaly of the elastic constant C_{33}^{Rhom} smears out near the crossing point to the structural transition. The phase diagram of Fig. 10 is consistent with the previous result obtained by resistivity measurements.[25]

In Fig. 11 we show the elastic constants of the $x=0.3$ compound with metallic properties. Here we take the rhombohedral geometry again. Around the ferromagnetic transition point $T_C=360$ K a small anomaly has been found in the elastic constant of C_{33}^{Rhom}. Even in the transverse mode C_{44}^{Rhom} and C_{66}^{Rhom} with E_g symmetry, no anomalous softening indicating quadrupolar fluctuation of the $d\gamma$ state has been found. This is contrast to the softening of the $(C_{11}-C_{12})/2$ mode in the compounds of $x=0.12$ and 0.165.

V. CONCLUDING REMARKS

In this paper we have made a systematic investigation of the elastic properties of the manganese compounds with the multiquantum degrees of freedom, spin, orbit, and charge. The elastic softening of the $(C_{11}-C_{12})/2$ mode above the structural phase transition point T_s is commonly observed for $x=0.12$ compounds of insulators and $x=0.165$ with colossal magnetoresistance. From the present experimental result, we conclude that the coupling of the quadrupolar moments O_2^0 and O_2^2 of the $d\gamma$ doublet in Mn^{3+} ions to the transverse $(C_{11}-C_{12})/2$ mode plays an important role for the quadrupolar ordering at the structural transition point. Furthermore, the absence of elastic softening in C_{44} above T_s in both $x=0.12$ and 0.165 compounds is also consistent with the absence of the O_{yz}-, O_{zx}-, O_{xy}-type quadrupolar moments for the $d\gamma$ state of Mn^{3+}. Even in the rhombohedral geometry softening of C_{44}^{Rhom} and C_{66}^{Rhom} above T_s in $x=0.165$ has been found. This result indicates that the quadrupolar effect of the $d\gamma$ doublet is relevant.

The quadrupole-strain interaction $|g_{\Gamma 3}|=10^2$–10^3 K for the $3d$ orbit of Mn^{3+} ions in both $x=0.12$ and 0.165 compounds is considerably larger than $|g_\Gamma|=10$–10^2 K in the $4f$ orbit in rare-earth compounds.[28–30] The relatively extended radius of the $3d$ orbit in the transition-metal ion is perturbed by a considerable amount by the quadrupolar field due to the acoustic wave. From the measurement of the softening of $(C_{11}-C_{12})/2$, we obtained the Jahn-Teller coupling energy $E_{JT}=Ng_{\Gamma 3}^2|\langle\varphi_{e_g}|O_{\Gamma 3}|\varphi_{e_g}\rangle|^2/\{(C_{11}^0-C_{12}^0)/2\}=52$ K for the compound of $x=0.12$ and $E_{JT}=15$ K for $x=0.165$. The present experimental result $E_{JT}=10$–10^2 K provides a criterion for the model calculation in the theoretical argument for colossal magnetoresistance.[18]

Elastic anomalies associated with charge ordering in $x=0.12$ and 0.165 compounds have been also found. The softening of $(C_{11}-C_{12})/2$ and C_{44} of $x=0.12$ above $T_{co}=145$ K indicates that the charge fluctuation modes with E_g and T_{2g} symmetry play an important role for the charge ordering. The investigation for the ordered structure of Mn^{4+} and Mn^{3+} ions below T_{co} by electron and x-ray scattering measurements is required.[18] In the case of $x=0.165$, a rounded anomaly of the bulk modulus C_B associated with the volume strain ε_B of A_{1g} symmetry is observed around the charge ordering point $T_{co}=100$ K. The symmetry breaking modes of $(C_{11}-C_{12})/2$ and C_{44} show few anomalies around T_{co} in $x=0.165$. This result suggests the glass character of

the charge-ordered states in $x=0.165$, which is caused by the incommensurability of Mn^{4+} ions to lattice periodicity and the considerable carrier density of the $d\gamma$ orbit in the ferromagnetic state.

The present ultrasonic study reveals many interesting phenomena associated with the coupling of the lattice degree of freedom to the quadrupolar moment of the $d\gamma$ doublet of Mn^{3+} ions as well as the charge fluctuation mode of Mn^{4+} ions. The electron-lattice interaction in the system $La_{1-x}Sr_xMnO_3$ gives rise to a structural change accompanied by the orderings of the orbit and charge degrees of freedom. The role of the electron-lattice interaction for colossal magnetoresistance is still an open problem. The isomorphous manganese compounds $Pr_{1-x}Ca_xMnO_3$ (Ref. 6) and $Nd_{1-x}Sr_xMnO_3$ (Ref. 31) with colossal magnetoresistance are also interesting systems where the electron-lattice interaction may play important roles. Ultrasonic experiments on these compounds are now in progress by our group.

ACKNOWLEDGMENTS

We wish to thank Professor M. Kataoka, Professor B. Lüthi, and Dr. S. Ishihara for valuable discussions and stimulating suggestions. This work was supported by a Grant-in-Aid for Scientific Research from the Ministry of Education, Science and Culture of Japan.

[1] G. H. Jonder, Physica (Amsterdam) **22**, 707 (1956).
[2] C. Zener, Phys. Rev. **82**, 403 (1951).
[3] P. W. Anderson and H. Hasegawa, Phys. Rev. **100**, 675 (1955).
[4] P.-G. de Gennes, Phys. Rev. **118**, 141 (1960).
[5] A. Urushibara, Y. Moritomo, T. Arima, A. Asamitsu, G. Kido, and Y. Tokura, Phys. Rev. B **51**, 14 103 (1995).
[6] Y. Tomioka, A. Asamitsu, H. Kuwahara, Y. Moritomo, and Y. Tokura, Phys. Rev. B **53**, 1689 (1996).
[7] J. B. Goodenough, Phys. Rev. **100**, 564 (1955).
[8] K. I. Kugel and D. I. Khomskii, Usp. Fiz. Nauk **136**, 621 (1982) [Sov. Phys. Usp. **25**, 231 (1982)].
[9] Y. Yamada, O. Hino, S. Nohdo, R. Kanao, T. Inami, and S. Katano, Phys. Rev. Lett. **77**, 904 (1996).
[10] J. Kanamori, J. Phys. Chem. Solids **10**, 87 (1959).
[11] R. Shiina, T. Nishitani, and H. Shiba, J. Phys. Soc. Jpn. **66**, 3159 (1997).
[12] S. Ishihara, J. Inoue, and S. Maekawa, Phys. Rev. B **55**, 8280 (1997).
[13] G. Matsumoto, J. Phys. Soc. Jpn. **29**, 606 (1970).
[14] Y. Murakami, J. P. Hill, D. Gibbs, M. Blume, I. Koyama, M. Tanaka, H. Kawata, T. Arima, Y. Tokura, K. Hirota, and Y. Endoh, Phys. Rev. Lett. **81**, 582 (1998).
[15] Y. Kino, B. Lüthi, and M. E. Mullen, Solid State Commun. **12**, 275 (1973).
[16] M. Kataoka and J. Kanamori, J. Phys. Soc. Jpn. **32**, 113 (1972).
[17] S. Hirotsu, J. Phys. C **10**, 967 (1977).
[18] A. J. Millis, R. Mueller, and B. I. Shraiman, Phys. Rev. B **54**, 5405 (1996).
[19] T. W. Darling, A. Migliori, E. G. Moshopoulou, S. A. Trugman, J. J. Neumeier, J. L. Sarrao, A. R. Bishop, and J. D. Thompson, Phys. Rev. B **57**, 5093 (1998).
[20] H. Fujishiro, M. Ikebe, Y. Konno, and T. Fukase, J. Phys. Soc. Jpn. **66**, 3703 (1997).
[21] T. J. Moran and B. Lüthi, Phys. Rev. **187**, 710 (1969).
[22] T. Goto, Y. Nemoto, A. Ochiai, and T. Suzuki, Phys. Rev. B **59**, 269 (1999).
[23] H. Kawano, R. Kajimoto, M. Kubota, and H. Yoshizawa, Phys. Rev. B **53**, 14 709 (1996).
[24] Y. Endoh, K. Hirota, S. Ishihara, S. Okamoto, Y. Murakami, A. Nishizawa, T. Fukuda, H. Kimura, H. Nojiri, K. Kaneko, and S. Maekawa, Phys. Rev. Lett. **82**, 4328 (1999).
[25] A. Asamitsu, Y. Moritomo, R. Kumai, Y. Tomioka, and Y. Tokura, Phys. Rev. B **54**, 1716 (1996).
[26] Y. Nemoto, H. Aoki, T. Goto, A. Ochiai, and T. Suzuki, Physica B **259-261**, 275 (1999).
[27] A. Loidl, R. Feile, and K. Knorr, Phys. Rev. Lett. **48**, 1263 (1982).
[28] P. Fulde, J. Keller, and G. Zwicknagl, Solid State Phys. **41**, 1 (1988).
[29] P. Thalmeier and B. Lüthi, in *Handbook of the Physics and Chemistry of Rare Earths*, edited by K. A. Gschneider, Jr. and L. Eyring (North-Holland, Amsterdam, 1991), Vol. 14, p. 225.
[30] S. Nakamura, T. Goto, S. Kunii, K. Iwashita, and A. Tamaki, J. Phys. Soc. Jpn. **63**, 623 (1994).
[31] H. Kuwahara, T. Okuda, Y. Tomioka, T. Kimura, A. Asamitsu, and Y. Tokura, in *Science and Technology of Magnetic Oxides*, edited by M. Hundley *et al.*, MRS Symposia Proceedings No. 484 (Materials Research Society, Pittsburgh, 1998), p. 83.